TEC-0014

AD-A257 301

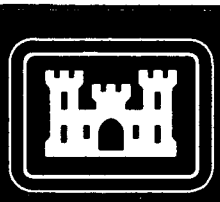

US Army Corps
of Engineers
Topographic
Engineering Center

T

E

C

Methods of Monitoring the Persian Gulf Oil Spill Using Digital and Hardcopy Multiband Data

Robert S. Rand
Donald A. Davis
M.B. Satterwhite
John E. Anderson

August 1992

92-28551

Approved for public release; distribution is unlimited.

U.S. Army Corps of Engineers
Topographic Engineering Center
Fort Belvoir, Virginia 22060-5546

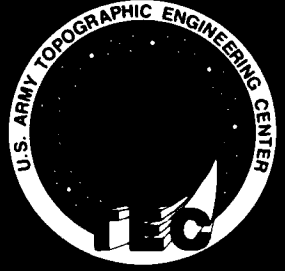

Destroy this report when no longer needed.
Do not return it to the originator.

The findings in this report are not to be construed as an official Department of the Army position unless so designated by other authorized documents.

The citation in this report of trade names of commercially available products does not constitute official endorsement or approval of the use of such products.

DISCLAIMER NOTICE

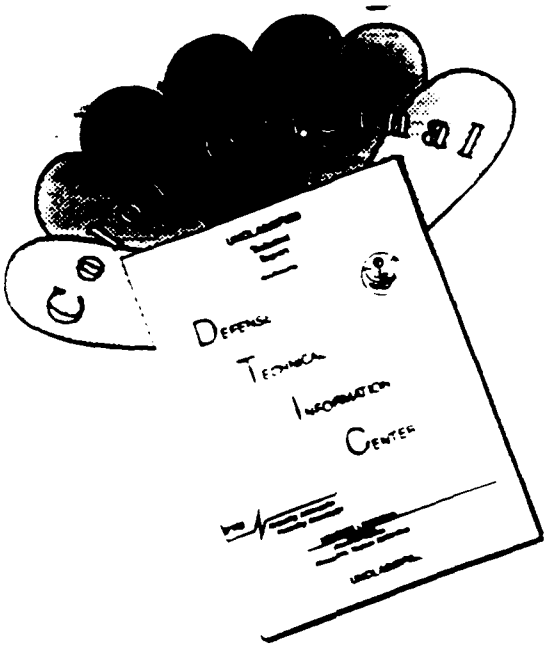

THIS DOCUMENT IS BEST QUALITY AVAILABLE. THE COPY FURNISHED TO DTIC CONTAINED A SIGNIFICANT NUMBER OF COLOR PAGES WHICH DO NOT REPRODUCE LEGIBLY ON BLACK AND WHITE MICROFICHE.

REPORT DOCUMENTATION PAGE

Form Approved
OMB No. 0704-0188

1. AGENCY USE ONLY (Leave blank)	2. REPORT DATE	3. REPORT TYPE AND DATES COVERED
	August 1992	Technical Report January - July 1991

4. TITLE AND SUBTITLE

Methods of Monitoring the Persian Gulf Oil Spill Using Digital and Hardcopy Multiband Data

5. FUNDING NUMBERS

6. AUTHOR(S)

Robert S. Rand M.B. Satterwhite
Donald A. Davis John E. Anderson

7. PERFORMING ORGANIZATION NAME(S) AND ADDRESS(ES)

U.S. Army Topographic Engineering Center
Fort Belvoir, VA 22060-5546

8. PERFORMING ORGANIZATION REPORT NUMBER

TEC-0014

9. SPONSORING/MONITORING AGENCY NAME(S) AND ADDRESS(ES)

10. SPONSORING/MONITORING AGENCY REPORT NUMBER

11. SUPPLEMENTARY NOTES

12a. DISTRIBUTION/AVAILABILITY STATEMENT

Approved for public release; distribution is unlimited.

12b. DISTRIBUTION CODE

13. ABSTRACT *(Maximum 200 words)*

A quick response demonstration was performed during the Persian Gulf War that showed a capability to monitor the path of oil dumped into the bay near Kuwait City using commercial satellite imagery. Both manual and semi-automated methods of image analysis were performed on AVHRR and Landsat TM imagery. Estimates of the oil area coverage were obtained using conventional classification methods. A hardcopy generation and reproduction capability was also demonstrated.

14. SUBJECT TERMS

Persian Gulf, Oil Spill, AVHRR, Landsat TM, Euclidean Distance, Bayesian Discriminant, Classifiers, Hardcopy Processing

15. NUMBER OF PAGES
45

16. PRICE CODE

17. SECURITY CLASSIFICATION OF REPORT	18. SECURITY CLASSIFICATION OF THIS PAGE	19. SECURITY CLASSIFICATION OF ABSTRACT	20. LIMITATION OF ABSTRACT
UNCLASSIFIED	UNCLASSIFIED	UNCLASSIFIED	UNLIMITED

CONTENTS

ILLUSTRATIONS

TABLES

PREFACE

This project was conducted to demonstrate a quick-response capability to monitor crisis situations using commercial satellite imagery. The requirement for such a capability became evident during the Persian Gulf War; particularly, the need for monitoring the path of the oil spill coming from oil dumped in the bay near Kuwait City. The Coast Guard's SLAR-based AIREYE sensor is usually deployed to major global oil spills. However, this system would have been too risky to operate because of the nature of the hostile environment.

The project was conducted during the period of January to July 1991. The most intense effort was made in the first two weeks of February 1991 during the war, in response to requests from the USACE Army Cold Regions Research and Engineering Laboratory and the Corps of Engineers Emergency Operation Center to monitor the Persian Gulf oil spill.

This was a laboratory effort initially involving TEC's Research Institute (RI), Space Programs Laboratory (SPL), and the Geographic Sciences Laboratory (GSL) to conduct the quick-response demonstration. Subsequently, TEC's Topographic Developments Laboratory (TDL) joined the effort, helping to formulate and demonstrate an improved quick-response capability via the prototype Quick Response Multicolor Printer (QRMP). Additional effort was also made by SPL to better characterize the performance of the semi-automated classifiers using the remotely sensed images.

The authors were the TEC team that conducted the quick-response demonstration. In addition, a special acknowledgement is made to Francis A. Ward, Chief, Graphic Systems Development Branch, who provided valuable support in formulating and demonstrating the improved quick-response hard copy capability.

The Space Programs Laboratory work was conducted under the supervision of Mr. Donald J. Skala, Chief, Exploratory Technology Branch; Mr. James E. Stilwell, Chief, Space Technology Division; and Dr. Joseph J. Del Vecchio, Director, Space Programs Laboratory. The Research Institute work was conducted under the supervision of Dr. Jack N. Rinker, Chief, Remote Sensing Division; and Mr. John V.E. Hansen, Director Research Institute. The Geographic Sciences Laboratory work was conducted under the supervision of Mr. Paul G. Logan, Chief, Data Base Development Branch; Mr. Douglas Caldwell, Chief, Terrain Analysis and Data Generation Division; and Mr. Bruce K. Opitz, Director, Geographic Sciences Laboratory. The Topographic Developments Laboratory work was conducted under the supervision of Mr. Francis A. Ward, Chief, Graphic Systems Development Branch; and Mr. Regis J. Orsinger, Director, Topographic Developments Laboratory.

Mr. Walter E. Boge was Director, and Colonel Kenneth C. Kessler was Commander and Deputy Director of the U.S. Army Topographic Engineer Center at the time of publication of this report.

METHODS OF MONITORING THE PERSIAN GULF OIL SPILL USING DIGITAL AND HARDCOPY MULTIBAND DATA

1.0 INTRODUCTION

1.1 Objective

The purpose of this effort was to demonstrate a quick response Corps of Engineers capability to detect and identify oil spills using commercial multiband satellite imagery, such as the Advanced Very High Resolution Radiometer (AVHRR) and Landsat Thematic Mapper (Landsat TM). The digital processing and analysis procedures needed to perform this task were to be identified, as well as the methodology for producing hardcopy products.

1.2 Background

A Remote Sensing team was assembled at the U.S. Army Topographic Engineering Center (TEC), comprised of members from TEC's Research Institute (RI), Space Programs Laboratory (SPL), and Geographic Sciences Laboratory (GSL), as a quick response to requests from the U.S. Cold Regions Research and Engineering Laboratory (CRREL) and the Corps of Engineers Emergency Operation Center to monitor the Persian Gulf oil spill (January-March 1991). Members of RI acquired the necessary image data, performed much of the visual image interpretation, and maintained a liaison among the various agencies. Members of SPL processed the data on the Space Research Test Facility, Multiband Image Processing System (SRTF/MBIPS), performing data screening, image classification (segmentation), and data reformatting for hardcopy processing. Members of GSL provided the quick-response hardcopy processing and output using the TIES/ERDAS, the electrostatic plotter, and the bubble jet copier.

Subsequently, SPL characterized in more detail the performance of the semi-automated image classifiers. Also, the Topographic Developments Laboratory (TDL) also worked with SPL in formulating and testing an alternate hardcopy production methodology utilizing the Quick Response Multicolor Printer (QRMP) prototype.

Imagery from two commercial satellite sensors was used; (1) the Advanced Very High Resolution Radiometer (AVHRR), and (2) the Landsat Thematic Mapper (Landsat TM). The AVHRR sensor generates data with 10-bit precision, 5 spectral bands, and pixels having an Instantaneous Field of View (IFOV) of 1.1 km. There are numerous satellites carrying this sensor. The spectral band widths vary according to the satellite and are listed in Table 1 (Section 2). Although the spatial resolution was a major disadvantage, the revisit cycle of a few times per day was a big advantage.

The Landsat TM sensor generates data with 8-bit precision, 7 spectral bands, and pixels having an IFOV of approximately 30 meters for all bands except Band 6, which has an IFOV of 120 meters. There are currently two Landsat satellites, each with a revisit cycle of 16 days. Typically, the revisit is once every 16 days, corresponding to a single satellite. However, if the two satellites are tasked to collect data over the same target in response to a time sensitive event, then the revisit time can be reduced to 8 days. The spectral bands are listed in Table 2 (Section 2.2).

1.3 Scope

The oil spill monitoring was accomplished using both AVHRR and Landsat TM imagery. The first scene processed was a 30 January 1991 Landsat TM image. The team members found no oil in this scene. Members later confirmed that the oil spill was actually to the north of the acquired scene. Because Landsat TM data could only be acquired every 8 days at best, a decision was made to acquire and analyze AVHRR data that was available for multiple times a day. A total of 16 scenes was processed on the SRTF/MBIPS covering the period between 16 January to 8 February 199. However, since 11 of the scenes were found to contain clouds over the region of interest, only 5 cloud-free AVHRR scenes were used in the analysis. Two additional Landsat scenes, taken on 8 February and 16 February, were subsequently processed and analyzed as they became available. Eventually, the main region of interest became the coastal waters near the Manifah Oil Fields, and the coastal towns of Jaziratal Batinah and Al Jubayl, Saudi Arabia.

This effort had essentially two aspects: Digital Processing and Analysis, and Hardcopy Product Support. Both manual and semi-automated digital processing techniques were used and are discussed in Section 2.0. Numerical results of the classification runs are presented in Section 3.0. Two methodologies of hardcopy production support were used, and are discussed in Section 4.0. Appendix A contains an example of the current status of Methodology II's capability. It should also be noted that all the photographs in this report were generated using the QRMP-prototype under Methodology II. Appendix B contains spectral curves of new and aged oil, as well as class statistics for the training sites used for the supervised classification algorithms. Appendix C contains processing-related data.

2.0 PROCESSING METHODS AND ANALYSIS

The Land Analysis System (LAS) software on the SRTF/MBIPS was used for the digital processing and analysis. This included inputing the data from 9-track tape, screening the data by displaying multiple band combinations of each scene, remapping 10-bit data to 8-bit AVHRR data, enhancing the image data, co-registering AVHRR scenes, and segmenting the AVHRR and Landsat image data using a number of alternative classifiers. The outputs from this processing included remapped subscenes suitable for hardcopy output; class maps of subscenes portraying oil, land, and water features; and oil area coverage estimates using the class map results.

2.1 AVHRR Processing and Analysis

A special purpose routine was used to input the AVHRR data.[1] The program enabled easy input of the 5-band/10-bit data as multiband image data. Because of the nature of its acquisition, some of the scenes were found to have a north-to-south orientation, and others had a south-to-north orientation. Therefore, a routine[2] was used to rotate the south-to-north scenes by 180 degrees. A smaller subscene containing the major portion of the Persian Gulf and coastal areas was generated for each of the five scenes.

The resulting five subscenes of AVHRR imagery were remapped from 10-bit data to 8-bit data by using a routine to generate multiband histograms,[3] manually identifying stretch points, and then using another routine[4] to perform a piecewise linear stretch. Table C1 in Appendix C lists the five names of the subscenes used and the corresponding mappings.

The five AVHRR subscenes were co-registered to each other by identifying tiepoints and and applying them in a sequence of registration-related routines.[5] Upon completion, all co-registration was achieved to an acceptable level (less than one pixel) with a translation and rotation transformation. The AV0124.MORN8 subscene was used as the base scene for which the other four subscenes were registered. During the registration process, these four subscenes were resampled using a bilinear interpolation option. As listed in Table C2, the names of these subscenes were given an additional "R" suffix (e.g. AV0116.NOON8 -> AV0116.NOON8R).

The co-registered subscenes were also saved as a 2X magnification for easy display and comparison. The magnified images were resampled using cubic convolution. As listed in Table C2, the names of these subscenes were given a "C" suffix (e.g. AV0116.NOON8R -> AV0116.NOON8C).

Each of the bands was visually analyzed by the team members. Based on the spectral band widths, listed in Table 1, and the thermal properties of oil as compared to water, it was

---

[1] LAS Routine LACIN.

[2] LAS Routine FLIP.

[3] LAS Routine PIXCOUNT.

[4] LAS Routine MAP.

[5] LAS Routines COORDEDT, TIEMERGE, NULLCORR, TIEFIT, and GEOM. A single program called REGISTER can generally replace the functions of TIEMERGE, NULLCORR, TIEFIT, and GEOM; however, instability of the statistical estimating parameters in the defining transformation required adjustment of the alpha acceptance values for a couple of the scenes . This option was not available in REGISTER.

anticipated that Band 4 or Band 5 (Long Wave/Thermal Infrared) would provide the most useful information, but that these would be redundant if used together. The team's observations confirmed this. Bands 1, 2, 3 were not useful for oil; although Band 3 readily showed strong heat sources, such as oil fires. In addition, 3-band color combinations were not found any more useful than Band 4.

Table 1. NOAA-AVHRR Sensor Band Widths

	Satellite Number	
Band Number	NOAA -6, -8, -10	NOAA -7, -9, -11, 12, -I, -J
B1	0.58 - 0.68 μm	0.58 - 0.68 μm
B2	0.725 - 1.10 μm	0.725 - 1.10 μm
B3	3.55 - 3.93 μm	3.55 - 3.93 μm
B4	10.50 - 11.50 μm	10.30 - 11.30 μm
B5	same as Band 4	11.50 - 12.50 μm

As a consequence of the initial observations, only Band 4 was used for the majority of the analysis. Figures 1 to 4 show photos of the AVHRR (Band 4) images. Figure 1, the January 16 image, can be used as a refe ence since there is no oil in the scene. Figure 2, the January 24 image, is a morning scene. At this time of day, since the oil is cooler than the water, it appears as a light snake-like feature off the coast, located about one-half to two-thirds of the way down the scene. Figure 3, the first of the February 1 images, is a morning scene. Once again, the oil is cooler than the water and appears as a light snake-like feature off the coast, but further down the scene. Figure 4, the second of the February 1 scenes, is an early afternoon scene. At this time of day the oil is heated by the sun, becoming hotter than the surrounding water, so it appears as a dark feature against the lighter water.

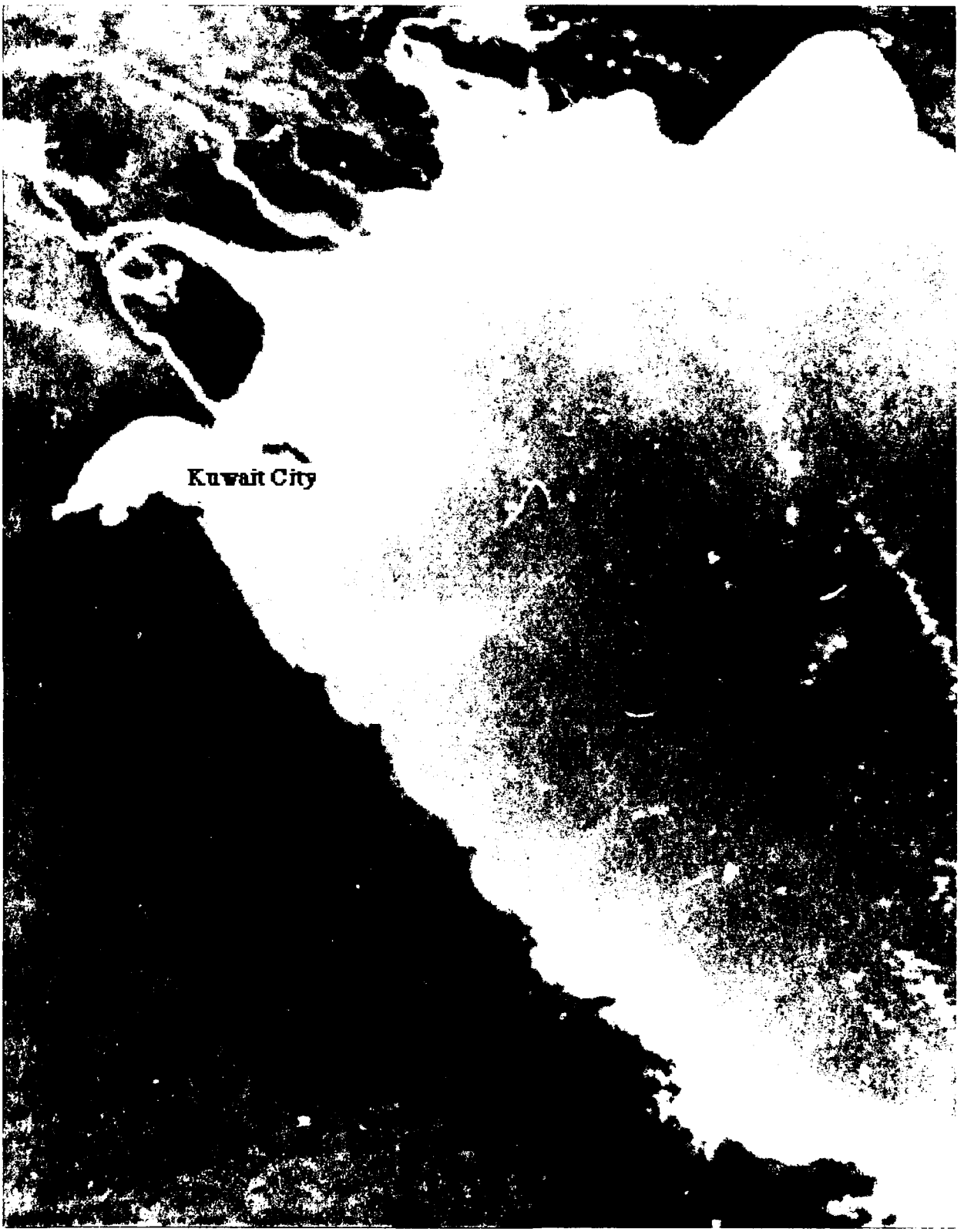

Figure 1. AVHRR (Band 4) -- January 16, 1991 -- NOON

Figure 2. AVHRR (Band 4) – January 24, 1991 – MORN

Figure 3. AVHRR (Band 4) – February 1, 1991 – MORN

Figure 4. AVHRR (Band 4) – February 1, 1991 – NOON

2.2 Landsat TM Processing and Analysis

The Landsat TM band widths are listed in Table 2. Spectral curves of fresh crude oil and weathered oil (floating oil, floating crude oil, and oil sludge) are shown in Appendix B. Given this information, the following framework can be postulated. Thermal Band 6 should show a good contrast between the oil and water because of temperature differences. Band 5 should show a good contrast between water and weathered oil, but not between water and fresh crude oil. Furthermore, along the coastal areas, where Band 1 should penetrate the water and scatter the light from underwater features (i.e. non-oil should be a lighter shade of gray), the oil should remain black.

Table 2. Landsat Thematic Mapper Bands

Band Number	Band Width
B1	0.45 - 0.52 μm
B2	0.52 - 0.60 μm
B3	0.63 - 0.69 μm
B4	0.76 - 0.90 μm
B5	1.55 - 1.75 μm
B7	2.08 - 2.35 μm
B6	10.4 - 12.5 μm

Landsat TM data was input using a general-purpose routine for ingesting tapes.[6] Usually, such data can be read using a special-purpose Landsat-ingest routine; however, the tape TEC received had a nonstandard 3-line blocking per record. This nonstandard blocking also made it impossible to read the data on other TEC systems.

Three dates of full-sized Landsat TM imagery were processed, 30 January, 8 February, and 16 February 1991 images. The scenes were predominantly water, with land only along the northern, western, and southern portions of the images. Each entire scene was screened visually using B6, B5, and B1 with emphasis on the northern edge and coastal edges, and the water-land boundary. Appropriate subscenes were generated from each image.

No oil was detected by the TEC team on the 30 January scene, and it was subsequently confirmed that no oil existed in the area at that time (it was located to the north). The team's analysis of the TM image required using several bands. Initially, some false alarms were raised as the team focused on some dark-tone linear features in B6, which stretched across portions of the scene. However, with the help of B1, which is sensitive to clouds, shadows, and atmospheric scattering these features were deduced to be thin clouds, shadows from thin clouds, or wind smoothing of the water. Using a priori spectral reflectance curves for new and aged oil (Appendix B), the team analyzed TM bands 1, 4, 5, and 7. They determined that previous reports of oil in this vicinity of the gulf were not correct and that the oil must still be north of the area covered by the Landsat TM scene. This conclusion was subsequently confirmed from the team's analysis of the AVHRR imagery and by other governmental agencies monitoring the gulf spill.

[6] LAS Routine IENTER.

Without using the visual bands, the confusion between oil and clouds is easily understandable. At times, both oil and clouds have similar thermal contrast with the water, and the lineal spatial patterns look amazingly similar to the pattern one would expect for oil. However, the situation becomes immediately apparent when incorporating Band 1. This band (blue) excels at showing haze along with clouds, both of which have bright responses in this band. Of course, oil has a black response in this spectral region. This concludes the argument, and eliminates any possible error between cloud patterns and oil.

Although oil was not present in this scene, a coastal site was selected, and a subscene of 1200 by 1200 pixels (33.6 by 33.6 km^2) was generated using the three multispectral bands B6, B5, and B1 (Red, Green, and Blue). Hardcopies of this imagery (generated using Methodology I) were produced to provide a control image in case future environmental impact studies were needed.

Oil was easily identified (visually) on the 8 and 16 February scenes using either B5 or B6. The oil spill on the 8 February image was present in the extreme northwest corner of the TM image, whereas on the 16 February image the oil had moved southward along the coast and was found over a large area (the latter is shown in Figures 5 to 7). Subscenes of 1200 by 1200 pixels containing the oil were generated. These were not co-registered because the drift in oil could not be contained within the same 1200- by 1200- pixel area, unless the scenes were resampled to a more coarse ground resolution. Such resampling and subsequent co-registration for both dates would have been time-consuming, and because of other priorities, these tasks were not performed.

Figures 5, 6, and 7 show photos of the Landsat images for the 16 February scene. Figures 5 and 6 illustrate the appearance of oil on Landsat Bands 5 and 6 (near IR and thermal). Notice the general agreement in the overall pattern of the oil in these two bands. However, there is a difference. B6 responds to temperature and is a useful indicator of the thickness of the oil, whereas, B5 seems to be indicating oil along certain shorelines.

What about this additional oil pattern along the shorelines? In particular, an apparent oil pattern can be seen along the western shore of Jaziratal Batinah, north of Al Jubayl (the cresent-shaped island in the center-right of image). According to B5, this feature may be oil, but it also may be wetland since many of the cove regions along the shoreline show about the same intensity response. The question is resolved by incorporating B1 which reveals that the areas in dispute are black and therefore oil. Figure 7 is a color composite showing the appearance in the three multispectral bands B6, B5, and B1 (Red, Green, and Blue).

Both the 8 and 16 February scenes were used in the classification studies. In addition to the two subscenes mentioned above, a larger portion of one of the scenes, 16 February, was resampled by a factor of 4 to reduce the size from 4800 by 4800 pixels to 1200 by 1200 pixels. The effective areal coverage of this scene was (134 by 134 km^2).

2.3 Classification Trials

Three classification algorithms were studied for their effectiveness in identifying oil: the Euclidean minimum distance classifier, the Bayesian discriminant classifier, and the ISODATA clustering method.[7] The Euclidean and Bayesian classifiers are supervised methods requiring training data. The ISODATA algorithm is an unsupervised method that requires no training data; however, its performance can often be enhanced by using a priori knowledge to define initial seed clusters. Table 3 describes the different trials in the experiment.

The Euclidean minimum distance classifier is simple and computationally fast. It is a linear classifier, meaning that the decision surfaces are hyperplanes. The decision function is

$$g_i(\mathbf{x}) = -r_i^2(\mathbf{x}) = -(\mathbf{x} - \mu_i)^t (\mathbf{x} - \mu_i)$$

where $\mathbf{x}$ is the n dimensional pixel vector being classified, and μ_i is the n dimensional mean vector for class ω_i. The function $g_i(\mathbf{x})$ is evaluated for each class, and the pixel is assigned to the class with the maximum value of $g_i(\mathbf{x})$.

Trials 2 to 8 were used to test the Euclidean minimum distance classifier as well as to determine if a subset of multispectral bands could achieve comparable results to all seven bands. This was done on the 16 February Landsat image. One variable that affects the performance of this classifier is the distance-threshold parameter. Under the MINDIST implementation, pixel vectors with a distance from each training vector that are greater than this threshold distance are assigned to a null class. During Trials 2 to 8 this parameter was varied. Selection of the thresholds was based on the class variance for each band using the expression

$$T = \text{sqrt}\left[\sum_{i=1}^{N} (r * \sigma_i)^2\right]$$

where N is the number of bands used in the classification (in this case either 4 or 7), r is a tunable parameter, and σ_i^2 is the class variance for band i. The value is interpreted as r times the standard deviation of class i. The value T was used as an initial guess, and then refined subjectively to improve the classification.

The Bayesian classifier is a quadratic algorithm that generates hyperquadric decision surfaces (i.e. hyperplanes, hyperspheres, hyperellipsoids, hyperparabloids). Accordingly, it is also more complex and computationally slower. From a statistical point of view, the algorithm is attractive because it weights the variables, and it accounts for correlation of the variables. Under the assumption that class data belong to multivariate normal populations, the method is optimal in the sense that it minimizes the probability of classification error. The multivariate normal (MVN) assumption allows the distributional properties of each class to be completely specified by a mean vector and covariance matrix. Unfortunately, violations of the MVN assumption (quite common in practice) and difficulties in estimating the class covariance matrices can potentially lead to poor performance.

---

[7] LAS routines MINDIST, BAYES, and ISOCLASS were used for the Euclidean minimum distance classifier, the Bayesian classifier, and the ISODATA clustering method, respectively. For a more complete discussion of these classifiers than what is given, see Charles W.Therrien. *Decision Estimation and Classification.* New York, NY: John Wiley & Sons, 1989.

The Bayes classifier appeals to the well-known Bayes Theorem and then uses the logarithm of the *a posterior* probability $f_{W|X}(\omega_i|x) = f_{X|W}(x|\omega_i) * P(\omega_i)$ as the definition of the Bayes discriminant function:

$$g_i(x) = -\frac{1}{2} * (x - \mu_i)^t \Sigma_i^{-1}(x - \mu_i) - \frac{1}{2} \log|\Sigma_i| + \log P(\omega_i) + \frac{n}{2} \log 2\pi$$

During this effort the a priori probabilities $P(\omega_i)$ are set equal and do not contribute to the decision. Since the last term is a constant that also does not contribute to the decision, the effective Bayes discriminant function used by the software is

$$g_i(x) = -\frac{1}{2} * (x - \mu_i)^t \Sigma_i^{-1}(x - \mu_i) - \frac{1}{2} \log|\Sigma_i|$$

In trials 9 and 10, the Bayesian classifier was tested on 4 bands and 7 bands of Landsat, respectively, for the 16 February image.

In trial 1, the ISOCLASS clustering method was tested on all the Landsat TM bands for the February 8 image. Similarly, during Trials 11, 12, and 13, the method was also tested on all the AVHRR bands for the 1 and 8 February images (see table 3).

The ISOCLASS method available under LAS is a slight modification of the well-known ISODATA (Iterative Self-Organizing Data Analysis Techniques A) algorithm developed by Ball and Hall.[8] This algorithm belongs to the category of clustering techniques that seek to minimize a specified objective function.

The ISODATA/ISOCLASS method is an iterative procedure, whereby clusters are continually split and merged. Achieving a local minimization of the objective function is easy, as it occurs when each of the samples in a data set has been assigned to the nearest cluster center. Such a solution is found at each iteration of the algorithm. However, a unique global solution for the data set cannot be guaranteed. This technique may settle into a local rather than global solution (the minimized value of its objective function is not a global minimum). The local solution generally depends on the initial starting estimates for the seed clusters and specifying different seed points for the initial clusters can produce different classification outputs. The differences may or may not be significant, but nevertheless a unique solution can never be guaranteed. Further discussion of the implementation can be found in an earlier TEC report.[9]

Prior to running the classification algorithms, a statistics file was generated for each scene, containing mean vectors and covariance matrices for numerous intermediate training classes. Eleven intermediate classes were defined for three types of oil (heavy, medium, light), three types of water, two types of land, wet cove, wet sand, and clouds. The same file was used for both supervised classifiers, and it was also used in one of the ISODATA trials (to define initial seed vectors). These eleven classes would subsequently be consolidated into seven classes as listed in Section 3.2, Table 5, and eventually to three classes (oil, water, land) as shown in Section 3.2, Figure 8.

---

[8] G.H. Ball, and D.J. Hall. *Isodata, A Novel Method of Data Analysis and Pattern Classification.* Stanford Research Institute Technical Report, (NTIS AD699616) Stanford, CA. 1965.

[9] Robert S. Rand. *A Hybrid Methodology for Detecting Cartographically Significant Features Using Landsat TM Imagery.* Fort Belvoir, VA: U.S. Topographic Engineer Center, ETL-0589, September 1991.

A 3-D scatterplot and further description of the classes is found in Section 3.2, Figure 9. The mean vectors and covariance matrices for this training set are listed in Appendix B, Tables B1 and B2, respectively. Signature plots of the mean vectors of oil (combined) and two water classes are shown in Figure B3.

Table 3. Classification Runs

TRIAL No.	IMAGE DATE	CLASSIFIER	TYPE IMAGE	SOURCE IMAGE	BAND COMBINATIONS
1	8-Feb-91	ISOCLASS	LANDSAT	SPILL2	1,2,3,4,5,6,7
2	16-Feb-91	MINDIST	LANDSAT	OIL216X4	1,2,3,4,5,6,7
3	16-Feb-91	MINDIST	LANDSAT	OIL216X4	1,5,6,7
4	16-Feb-91	MINDIST	LANDSAT	OIL216X4	1,2,3,4,5,6,7
5	16-Feb-91	MINDIST	LANDSAT	OIL216X4	1,5,6,7
6	16-Feb-91	MINDIST	LANDSAT	OIL216X4	1,2,3,4,5,6,7
7	16-Feb-91	MINDIST	LANDSAT	OIL216X4	1,5,6,7
8	16-Feb-91	MINDIST	LANDSAT	OIL216X4	1,2,3,4,5,6,7
9	16-Feb-91	BAYES	LANDSAT	OIL216X4 W = (1 1 1024 1024)	1,5,6,7
10	16-Feb-91	BAYES	LANDSAT	OIL216X4 W = (88 88 1024 1024)	1,2,3,4,5,6,7
11	1-Feb-91	ISOCLASS	AVHRR	AV0201.NOON W = (200,140,70,30)	1,2,3,4,5
12	1-Feb-91	ISOCLASS	AVHRR	AV0201.NOON W = (200,140,70,40)	1,2,3,4,5
13	8-Feb-91	ISOCLASS	AVHRR	AV0208.NOON W = (540,370,40,30)	1,2,3,4,5

Figure 5. Landsat TM (Band 5) – February 16, 1991

Figure 6. Landsat TM (Band 6) – February 16, 1991

Figure 7. Landsat TM (Composite) – February 16, 1991

3.0 CLASSIFICATION RESULTS

3.1 Oil Coverage Estimates

The estimates from the classification trials of the oil area coverage are listed in Table 4 and illustrated by a class map in Figure 8. Because of the lack of ground truth for this project, only a subjective comparison of the performance of the classifiers could be made visually. The nature of the problem (moving oil, particularly in a wartime environment) is such that ground truth is not likely ever to be available. In fact, a controlled study that delineates exact reference locations of moving oil in water is extremely difficult and rather costly to implement, even under ideal circumstances.[10] However, the nature of the problem (oil in water) is also such that most classification errors are easy to identify visually. For example, the presence of oil within interior land masses would be an obvious error.

Table 4. Classification Results

TRIAL No.	CLASSMAP NAME	SIZE	THRESHOLDS	OIL Coverage (km^2)
1	SPILL2.ISOCLASS	1024 X 1024		17.95
2	OIL216X4.MDIST	1200 X 1200	none	100.69
3	OIL216X4.MDIST2	1200 X 1200	30 for all classes	119.62
4	OIL216X4.MDIST3	1200 X 1200	30 for all classes	104.47
5	OIL216X4.MDIST4	1200 X 1200	20 for Oil, 30 for others	103.68
6	OIL216X4.MDIST5	1200 X 1200	55 for all classes	117.42
7	OIL216X4.MDIST6	1200 X 1200	25 for Oil, 30 for others	111.21
8	OIL216X4.MDIST7	1200 X 1200	35 for Oil, 55 for others	107.40
9	OIL216X4.BAYES	1024 X 1024		Uncertain
10	OIL216X4.BAYES2	1024 X 1024		Uncertain
11	AV0201.ISO	70 X 30		171.00
12	AV0201.ISO2	70 X 40		104.00
13	AV0208.ISO	40 X 30		40.00

3.2 Classifier Performance

In general, the Euclidean classifier produced results that were consistent among themselves and with visual observations. Trials 7 and 8 produced the best of the minimum distance results. Regarding missed oil, very few pixels visually observed as oil were misclassified as water. Regarding false alarms, only a handful of pixels visually observed on the land were misclassified as oil. The four-band combination B1, B5, B6, B7, produced essentially equivalent results as the seven-band combination.

The ISOCLASS clustering performed in Trial 1 actually produced better results for this date imagery. However, initial optimism was quickly shattered when the algorithm was applied to other scenes with very unstable results. For example, a comparison of the oil coverage for Trials 11 and 12 using AVHRR data shows a coverage of 171 km^2 vs. 104 km^2. The Trial 11 output drastically overestimated the amount of oil. However, the only

[10] Some studies using passive microwaves have been conducted. One such effort is documented in James Hollinger; *Determining Oil Spill Thickness Using Passive Microwaves*; Naval Research Laboratory; 1974.

distinguishing difference between runs was a slight change in the size of the images from 70 by 30 pixels to 70 by 40 pixels, which added an additional strip of water. The rationale for this behavior is the potential problem of the ISOCLASS solution becoming trapped in a local minimum and unable to reach the global minimum, as was discussed in Section 2.3.

The Bayesian discriminant classifier trials generated mysterious results that are difficult to interpret. From a theoretical standpoint, the Bayesian approach is preferable over the Euclidean distance. The latter is most appropriate if all the variances are equal and the variables are independent. The Bayesian method accounts for unequal variances and the lack of independence, and it models the size and shape variations in the training class distributions. It is also a statistically optimal classifier if the assumed multivariate normality of class data is correct (see Section 2.3). Accordingly, the Bayesian classifier should provide more accurate results than the Euclidean distance classifier. Generally, the experience reported in the literature is in keeping with this expectation and the Bayesian classifier is generally viewed as providing better overall results than the Euclidean distance classifier.

In apparent conflict with this rationale, the results of Trials 9 and 10 indicated a far greater amount of oil than that of the Euclidean minimum distance classifier or the ISOCLASS clustering algorithm that could not be confirmed visually. Both Oil H and Oil M had such troublesome areas. A post-processing operation was subsequently performed on the Bayesian results that relabeled samples outside a specified threshold into an unknown class.[11] Numerous thresholds were specified; however, the various thresholds had one of two effects. Either the detected oil samples remained unchanged or the majority of the scene was relabeled as a null class. The four-band combination, B1, B5, B6, B7, produced essentially equivalent results as the seven-band combination for the Bayesian classifier and the thresholds.

Was this detection of additional oil correct or false? During the demonstration, the analysts acted cautiously and dismissed the Bayesian results as erroneous. They could not visually identify the oil in these apparently extraneous regions using any of the Landsat TM band combinations, and although the extraneous Oil M regions had a certain amount of spatial structure, much of the extraneous Oil H regions appeared somewhat random. Unfortunately, the lack of ground truth made it impossible to reach a definite conclusion.

If these additional detections were incorrect, a possible explanation lies in the covariance structure of the training data. A comparison of the covariance matrices of water as compared to oil (listed in Appendix B, along with the mean vectors) shows that water is a tightly defined class as compared to oil. The variances of concern range as follows:

Water A	.02	to	0.64
Water B	.04	to	2.34
Oil H	.48	to	23.19
Oil M	.41	to	134.83
Oil R	.89	to	58.93

In particular, the variances of Water A are likely to be problematic, since they are all less than one (0.64, 0.26, 0.05, 0.08, 0.02, 0.31, 0.10 for bands 1 to 7, respectively). The variances of Water B are not that much better (2.34, 0.19, 0.11, 0.22, 0.04, 0.61, 0.25 bands 1 to 7, respectively).

[11] LAS Routine UNKNOWN.

Figure 8. Class Map Generated from Landsat TM.

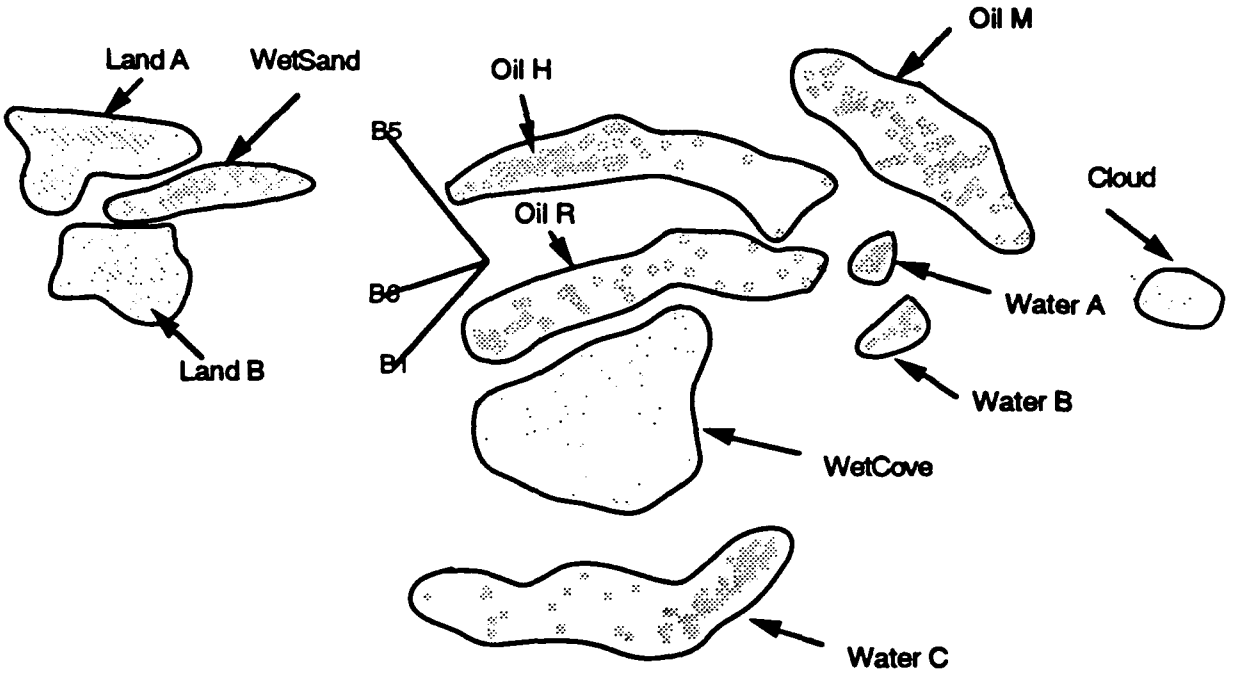

This is one projection of a three-dimensional scatterplot of the training data. Each training set is portrayed as a cluster (or cloud of data). Such scatterplots allow an analyst to anticipate the cluster shape of the underlying population distributions, and also to observe any overlap between the clusters. The program that generates this plot allows the user to spin the 3-D axis to view the data from any direction.

Geographically, Water A and Water B are at large distances from the shoreline and presumably in deep water, whereas, Water C is an off-shore water sample. WetCove is along the shoreline in a cove, and presumably heavily saturated with water. WetSand is located quite a distance inland.

According to this diagram, each of the classes appears to be separable. Rotating the plot would show that all the classes are indeed well separated, even though some, such as WetSand and Land B, appear to be close in this projection.

Figure 9. 3-D Scatterplot Results for B1, B5, B6.

If multivariate normality is assumed, then from a statistical viewpoint at least 95 percent of the water pixels would vary only a fraction of one gray shade from its class mean. Of course, the imagery is quantized to integer values and fractional data do not exist. Since the Bayesian classifier assumes multivariate normality and uses the covariance matrix in defining a distance metric (the Euclidean distance does not), it is very plausible that this classifier could mislabel legitimate water pixels as oil.

The scatterplot projection shown in Figure 9 also shows a tightly-defined water class and broadly-defined oil classes, and in addition, shows these classes to have a close pairwise distance as compared to other class pairs. Notice that Oil H contains a couple of apparent outliers, which should probably have been reassigned: one to Oil M and the other to Oil R. As it is defined (with these two pixels included), the estimate for the covariance of Oil H is exaggerated, and the modeled distribution is wider than it probably should be. Software limitations at the time prevented this issue from being explored further; however, it is being researched currently at TEC. Although it is beyond the scope of the effort to elaborate

much further, the results indicate that the presence of outliers in a training class can indeed greatly exaggerate covariance estimates. This explanation offers another way for water pixels to be misclassified as oil.

Noting these arguments, it is interesting to observe the results of the auto-classification trial that was subsequently performed using the Bayesian and Euclidean classifiers. The results, as listed in Table 6, show the Bayesian classifier performed flawlessly with 100 percent accuracy on the prototype data. This is in spite of the suspicious covariance structure. However, it is worth mentioning that TEC researchers have noticed this type of behavior in other studies.[12] Unfortunately, training data can often produce excellent autoclassification results, but have serious problems in classifying other portions of a scene.

It would then seem reasonable to conclude that the Bayesian classifier performed poorly on this data set. However, a closer look at the Bayes class map revealed that although the Oil H regions appeared somewhat random, the Oil M pattern seemed to radiate away from the oil identified by the other classification trials. A thin layer of oil would most definitely act this way.

Is it possible that the Bayesian classifier might be detecting a thin sheet of oil otherwise invisible -- oil that was not detected using the minimum distance or ISODATA methods, and that also was not noticed visually? Although not part of this quick-response effort, additional statistical analysis and classification trials were subsequently performed. Results from this follow-up analysis showed that combining the Water A and Water B classes succeeded in making the class covariance broader with only a minor affect on the class means. This action improved the visual appearance of the resulting image classification. Most of the troublesome Oil H was replaced as Water. The random patterns vanished almost completely.

However, essentially all of the troublesome Oil M areas remain. Closer visual analysis focusing on these areas indicated that indeed there may be something after all that looks like oil. These areas have a pattern that would resemble a thin oil sheet. The areas are located near the shoreline and the Band 1 pattern is dark, not as black as the known oil areas, but it does seems to be obscuring underwater features that should be seen. Since the investigators cannot reach a solid conclusion based on visual analysis, perhaps it is not surprising the Bayesian algorithm performed as it did. At the very least, it must be said that the Bayesian algorithm focused the investigators attention on an area that otherwise would have been overlooked.

Another effort is being conducted to study the effect of modifying the Bayesian algorithm by invoking a minimum-variance criterion and chi-squared distance rejection threshold.[13] Initial results are promising. In particular, by invoking a minimum-variance criterion, problems of misclassifying water samples as something else are greatly reduced. The chi-squared rejection criteria is proving useful to reduce errors by incorporating a null class; thereby allowing samples that were forced into a category by default to be rejected from the default class and relabeled as null. Unlike the LAS implementation that was used unsuccessfully in this effort, the criteria proposed seems to work without assigning almost everything to a null class.

---

[12] Robert Rand and Donald Davis. *Interactive Multivariate Analysis Techniques to Extract Natural and Man-Made Features from Broad-Band Spectral Imaging Data.* Fort Belvoir, VA: U.S. Topographic Engineer Center, in publication.

[13] Ibid.

Table 5. Consolidated Class Conversions

To assess the actual performance for either the complete scenes or the auto-classification runs, the original eleven training classes were consolidated into seven classes as follows:

Consolidated Class	Original Class(s)
Class 1 = Oil H	Oil H
Class 2 = Oil M	Oil M
Class 3 = Oil R	Oil R
Class 4 = Land	Land A, Land B
Class 5 = Wetland	WetCove, WetSand
Class 6 = Water	Water A, Water B, Water C
Class 7 = Clouds	Clouds

Table 6 . Auto-Classification Results for Seven Bands.

The Bayesian discriminant and Euclidean minimum distance classifications were performed using 11 training classes with means and covariance as shown in Appendix B. The statistics were gathered from the prototypes and the classification was performed on the same data. After the classifications were completed, these 11 classes were combined into 7 classes as listed in Table 8. Each row represents the percentage of class labels assigned to each training class. Read across (e.g. for the Euclidean results, and for the Oil M prototypes, 81.33% were classified correctly; 9.33% were incorrectly labeled as Oil H; and 9.33% were incorrectly labeled as Water).

BAYES CONTINGENCY RESULTS - Training Data = oil216_protos7

Class	1	2	3	4	5	6	7
1	**100.00**	0.00	0.00	0.00	0.00	0.00	0.00
2	0.00	**100.00**	0.00	0.00	0.00	0.00	0.00
3	0.00	0.00	**100.00**	0.00	0.00	0.00	0.00
4	0.00	0.00	0.00	**100.00**	0.00	0.00	0.00
5	0.00	0.00	0.00	0.00	**100.00**	0.00	0.00
6	0.00	0.00	0.00	0.00	0.00	**100.00**	0.00
7	0.00	0.00	0.00	0.00	0.00	0.00	**100.00**

EUCLIDEAN CONTINGENCY RESULTS - Training Data = oil216_protos7

Class	1	2	3	4	5	6	7
1	**95.77**	4.23	0.00	0.00	0.00	0.00	0.00
2	9.33	**81.33**	0.00	0.00	0.00	9.33	0.00
3	0.00	2.17	**89.13**	0.00	0.00	8.70	0.00
4	0.00	0.00	0.00	**100.00**	0.00	0.00	0.00
5	0.00	0.00	0.00	3.73	**96.27**	0.00	0.00
6	0.00	0.00	0.00	0.00	0.36	**99.64**	0.00
7	0.00	0.00	0.00	0.00	0.00	0.00	**100.00**

4.0 HARDCOPY REPRODUCTION

Two methodologies for hardcopy reproduction were used in this effort. Methodology I provided an immediate response to the quick-response requirement, and provided a very acceptable product that was well received in the community. However, it was not the most desirable solution, since the process had an extra layer of processing for defining the final radiometric adjustments, and the plotter used was best suited for graphic plotting rather than photographic printing. Methodology II was subsequently formulated and tested after the quick-response requirement was satisfied.

4.1 Methodology I

This methodology provided an immediate response to the quick-response requirement. It is discussed in the manner it was implemented during the demonstration.

4.1.1 Scene Processing

Digital scenes for hardcopy processing were subset into 1024 by 1024 blocks on LAS using the AVHRR and Landsat TM data depicting the spill as it made landfall in coastal Saudi Arabia. The tapes were generated as band-interleaved by line (BIL) composite images (rasters) and passed to the Earth Resource Data Analysis (ERDAS) image processing system. The ERDAS system is networked via TCP/IP to a SUN Sparcserver 490. Also configured as a node on the network is a large format (D and E size) Precision *Image color electrostatic plotter*. This plotter was used to create graphics at a scale of approximately 1:50,000 of the spill area.

Scenes generated on the LAS were pre-processed using the ERDAS software before plotting. The program executed to bring the data into the Sparcserver's disk was "**dd**" under the UNIX operating system. Each raster image was read from tape, and a statistics file was generated to collect and preserve the image statistics generated by LAS of the original image data sets. Image statistics representing spectral enhancements used for hardcopy production were generated using ERDAS.[14] This program allows an enhanced scaled data set to be written out as a file, and permits the custom application of algebraic expressions to multiple or single band files. Since the plotter renders images using cyan, magenta, yellow, and black (CMYK) and the 8- bit rasters are stored as red, green, and blue (RGB), it was essential that the histogram data be collected and applied to the image files as color look-up tables and be output as the digital file to be plotted. Spectral enhancements developed and written out as plot files served two purposes: (1) Oil in the scene was more obvious after histogram adjustment, particularly where band 1 in TM was used, and (2) Resulting hardcopy plots were brighter and were more representative in color to the same images on the video display.

4.1.2 Hardcopy Production

The new raster images were examined[15] to check for any anomalies in the data, i.e. pixel drop-out, swapped lines and samples, color integrity, etc., before the next phase of processing prior to plotting. All lines and samples were determined to be acceptable, and

[14] ERDAS routine **ALGEBRA**.
[15] ERDAS routine **READ**.

RGB to CMYK conversion was initiated to generate formatted plotfiles to be passed to the plotter. To accomplish this, software[16] was used to format and place the rasters in PI-CGI raster graphics format. In addition, legend, scaling, and boundary options within the software allowed customization of the resulting plot files. Some loss of chroma and color values took place in a few of the images. This was due mainly to limitations in the electrostatic process used for rendering the images. Cartographic plotters are intended mainly for line, point, and polygonal data sets - not dense image (photographic-type) data sets. Dense rasters, reproduced at 100 to 400 dots per inch, lose some quality and detail through resampling and data compression. Additionally, the RGB to CMYK conversion can corrupt color values depending on the plotter used, media, humidity, temperature, and the mechanical process.

Thirteen graphics were produced for scenes acquired on the 1st, 8th, and 16th of February 1991. The AVHRR full-resolution scenes covered the entire Persian Gulf region and border countries. Scenes generated from Landsat TM were full-resolution mosaics covering the eastern border of Kuwait (Mina az Zawr), south of the Manifah oil fields over coastal Saudi Arabia to Ra's az Zawr. Each graphic took approximately 25 minutes to plot, once the files were pre-processed to place them into PI_CGI format. Plotting time can be varied, and it was determined that it was more advantageous to plot slower since the plot files were dense raster files greater than 5 megabytes. Plot time variability is determined by ***writing*** (placing the electrically charged image on the media) and ***toning*** (painting the charged image with color toner solution). These operations can be done simultaneously for faster plotting, or separately for slower plotting.

Once the original graphics were produced, multiple reduced copies were reproduced using two Canon BubbleJet copiers.

4.2 Methodology II

Subsequent to Methodology I, a different method for reproducing hardcopy was developed that improved the appearance of the images on hardcopy and increased annotation flexibility. Since this method also reduced the processing steps and the printing time was faster, it should be quicker and less expensive.

4.2.1 Scene Processing

After the image-screening process is completed on LAS, the scenes of interest are transferred via the Ethernet from the LAS to the Macintosh II workstation. Single-band gray shade or three-band color combinations can be used. If linear piecewise radiometric remappings are desired to improve the visual appearance of the scenes, this operation should be applied prior to the transfer.

Once the transfer is completed, the image data is read and processed by a commercially written Macintosh image/photo processing program.[17] All the necessary image cropping, annotation, and final radiometric adjustment operations are performed interactively with the program. The Macintosh II workstation and software used in the process perform 32-bit color operations, and therefore provide full true-color support. The resulting digital image that the analyst views, prior to hardcopy generation, is exactly what the analyst gets. An almost identically-configured system exists as the interface to the Quick-Response Multicolor Printer (QRMP) prototype that is used for hardcopy output.

---

[16] PIMAGE software

[17] Adobe Photoshop, Version 2.0.

The images are ingested as raw data and converted into their own multichannel format. Upper limits on the input multichannel image data have not yet been established, although 2560 pixels by 5632 lines have been successfully manipulated (a 3-channel color 42MB file). The presently established upper limit on the output images is a total of 24 MB for a multichannel scene. This is not a limitation of the image/photo processing software, but rather a memory limitation of the copier, which will soon be resolved by new memory boards.

Once the scene has been processed to the desired level, photographically, two additional parameters must be specified. These parameters are the page size and the print density in dots-per-inch (dpi). Available page sizes are the standard letter (8.5" by 11") and tabloid size (11" by 17"). The print density ranges from 72 dpi to 400 dpi. Of course, the density setting affects both the scale of the imagery and the size of the image that can be printed. For example, at a density of 72 dpi, only an image of 648 by 936 pixels could be printed on a 9- by 13- inch area within a tabloid-sized sheet of paper. At 200 dpi, an image of 1800 by 2600 pixels could be printed on the same-sized area.

The file can be saved as a raw data file, a PICT data file, or a program-specific data file. However, if one wishes to save the print parameters, the program-specific format should be used. The file is then copied to either a 1.4 MB floppy disc, or 45 MB removable cartridge, depending on the file size.

Note that because identical software exists on the QRMP, much of this scene processing could be performed directly on the QRMP as well. Convenience and user expertise should determine this.

4.2.2 Hardcopy Production

As mentioned above, an almost identically-configured system exists as the interface to the Quick-Response Multicolor Printer (QRMP) prototype that is used for hardcopy output. Therefore, the disc file, created by *Scene Processing*, is read directly into the QRMP prototype system. The same program used to create the file is executed, the file is opened, and the print command is issued.

Each of the two QRMP prototypes is a network system presently consisting of a Macintosh IIfx, a Raster Input Processor (RIP), a Cannon CLC500 copier/printer, and a Canon BubbleJet copier. The Macintosh files are transferred to the RIP, which converts the image files into a PostScript file that the CLC500 printer can interpret. The output of the CLC500 is a letter or tabloid-size photo. These photos are then copied with some magnification factor (1x to 12x) using the BubbleJet copier. The format of the BubbleJet allows the copies to have a maximum size of 20 by 30 inches.

Noting the original pixel size (e.g. Landsat TM has a resolution of 28 meters/pixel), the print density recorded by the laser printer, and the scale factor introduced by the BubbleJet copier, one can determine the scale factor of the resulting hardcopy output. Typically, one determines the scale factor in advance, noting the image pixel size and adjusting the print density of the printer and the scale factor of the copier accordingly.

All of the photos in this report were generated using Methodology II. Except for the figure in Appendix A, annotation of the photos was given only limited attention, because of the limited resources available after the Quick-Response demonstration. Also, to reduce cost, only a standard grade of paper was used. The best representation of the capabilities of the system is illustrated in Appendix A, where annotation/graphics was given greater emphasis, and a much higher grade of (clay-based) paper was used.

Update on Production Methodology II. Since this effort was completed, a direct digital interface from the Macintosh/RIP to the Canon BubbleJet copier/printer was established. This will be particularly useful for generating poster-size prints directly from a digital file, eliminating the need for the intermediate step of generating a page-size (letter or tabloid) print that must be subsequently magnified.

5.0 CONCLUSIONS

Oil was identified on both AVHRR and Landsat TM. The success in using AVHRR was primarily due to the contrast between oil and water in the thermal wavebands, and to the massive amounts of concentrated oil. As the oil became dispersed on the later dates, it was far more difficult to detect, because its thermal signature became merged with that of the coastal features. Much of the oil was missed. However, this same oil was easily identified on the Landsat scene of the corresponding date because of the increased spatial resolution. Also, automated detection became possible because of additional bands.

Subsets of the most useful AVHRR and Landsat TM bands for detecting and identifying oil were easily determined. The useful AVHRR bands were B4 and B5. Only one of these is needed, and the team members used B4.

The most useful Landsat TM bands were B6, B5, and B1. Although Landsat TM B6 was perhaps the most important for conservative oil estimates, B5 possibly indicated additional oil near shorelines. The B1 band was essential to eliminate possible confusion between oil and wetland, between oil and cloud patterns, as well as between oil and near-shore bathymetric features.

Both manual methods and interactive classification routines were successful in identifying the oil. Manual methods served best for screening the data, determining the best band combinations, and verifying the actual presence of the oil. Manual interpretation of AVHRR was essential because of the limited spatial resolution and the limited number of useful spectral bands.

Interactive routines were useful in generating class maps and providing oil area coverage estimates. The best conservative estimates were achieved using a simple minimum distance classifier with threshold bounds for a null class. A four-band combination, B1, B5, B6, B7, produced essentially equivalent results as the seven-band combination.

The unsupervised ISOCLASS technique produced some successful results; however, it was also found to be unstable. Excellent results deteriorated to nonsense with only a small change in scene content.

The results of the Bayesian discriminant classifier applied to the Landsat TM scene produced results that were difficult to interpret and raised some important issues. Some of the difficulty was traceable to tightly-defined water classes (i.e. very small variances in the class covariance matrix), and possibly to prototype outliers in one of the oil classes.

There is the need for software that can adapt to the problems associated with tightly-defined classes, and for software that detects and eliminates outliers in training data. These problems can often be avoided through skillful selection of training data; however, the required talent is probably beyond the level that should be expected of the average user, and software should be developed to circumvent these problems.

Overall, the classification results demonstrated successes and shortcomings that were in keeping with those of other studies conducted by TEC researchers evaluating multispectral data with different scene content. An ongoing effort is addressing the shortcomings for the generalized problem (any scene content).

A study should be performed that assesses the potential for using Landsat or other spectral imaging data along with semi-automated machine algorithms for the specific problem of detecting thin layers of oil. The Bayesian classifier might have detected such layers using Landsat TM; however, the lack of ground truth available in this effort made it impossible to reach any definite conclusion.

A quick response time of 24 hours was achieved for responding to emergency operations, as measured from the moment TEC received the data tapes to completion of hardcopy plotter products, and areal oil coverage estimates. Subsequent to the demonstration, a methodology utilizing the Quick-Response Multicolor Printer Prototype (QRMP) for producing better quality hardcopy products with an equivalent (or better) response time was formulated and tested.

Most of the photos in this report do not fully represent the true capability of Methodology II. Because of the limited resources available after the Quick-Response demonstration, efforts were directed at printing the scenes in this report with only limited annotation. The print quality is also somewhat limited because of paper quality (clay-based paper should be used). A more representative sample of the capabilities of the system is illustrated in Appendix A. Such a photo could easily be enlarged to 20 by 30 inches using the BubbleJet copier.

6.0 REFERENCES

Ball, G.H. and Hall D.J. *Isodata, A Novel Method of Data Analysis and Pattern Classification.* Stanford Research Institute Technical Report, (NTIS AD699616) Stanford, CA. 1965.

Hollinger, James; *Determining Oil Spill Thickness Using Passive Microwaves*; Naval Research Laboratory; 1974.

Rand, Robert S. *A Hybrid Methodology for Detecting Cartographically Significant Features Using Landsat TM Imagery.* Fort Belvoir, VA: U.S. Topographic Engineer Center, ETL-0589, September 1991.

Rand, Robert and Davis, Donald. *Interactive Multivariate Analysis Techniques to Extract Natural and Man-Made Features from Broad-Band Spectral Imaging Data.* Fort Belvoir, VA: U.S. Topographic Engineer Center, in publication.

Therrien, Charles W. *Decision Estimation and Classification.* New York, NY: John Wiley & Sons, 1989.

APPENDIX A: Kuwait Airport and Oil Fires


Map Data from
JOG-A, NH 38-12
on ADRG CD-ROM
racetrack
quarry
hospital
building
quarry
quarry
KUWAIT
INTERNATIONAL
radio
receiver
station
water
tanks
army barracks
quarry
building
numerous
oil wells
quarries
oil
wells
pylon
410
gathering
centre
gathering centre
numerous
oil wells
Landsat Image
Bands 5, 4 & 1 (RGB)
Date of Image
22 Feb. 1991
Band 6 (Thermal) shows location of
individual oil well fires

APPENDIX B: Spectral Curves and Statistics

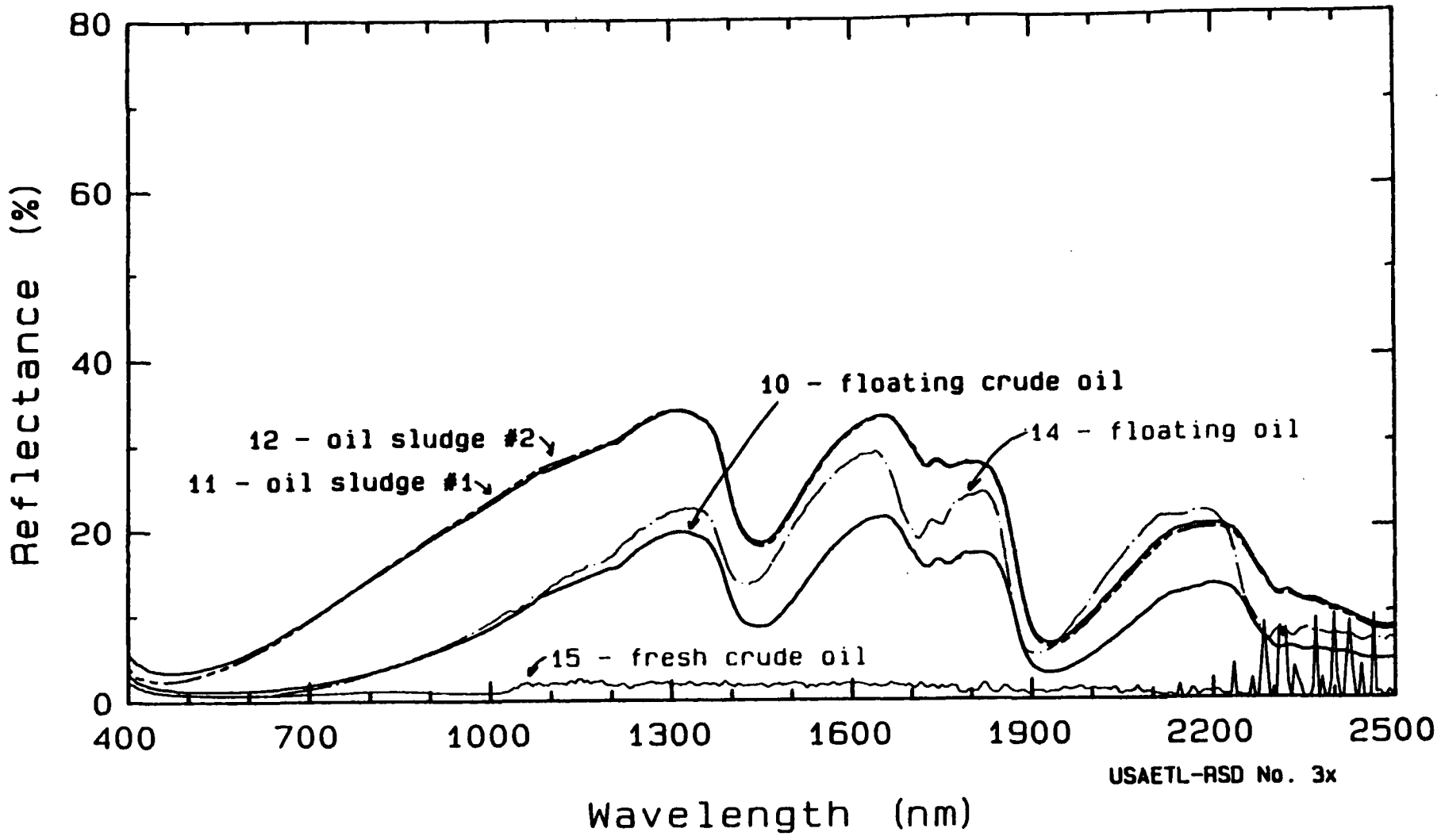

FIGURE B1. Spectra of Fresh and Weathered Oil Alaska Oil Spill, Jan 1990.

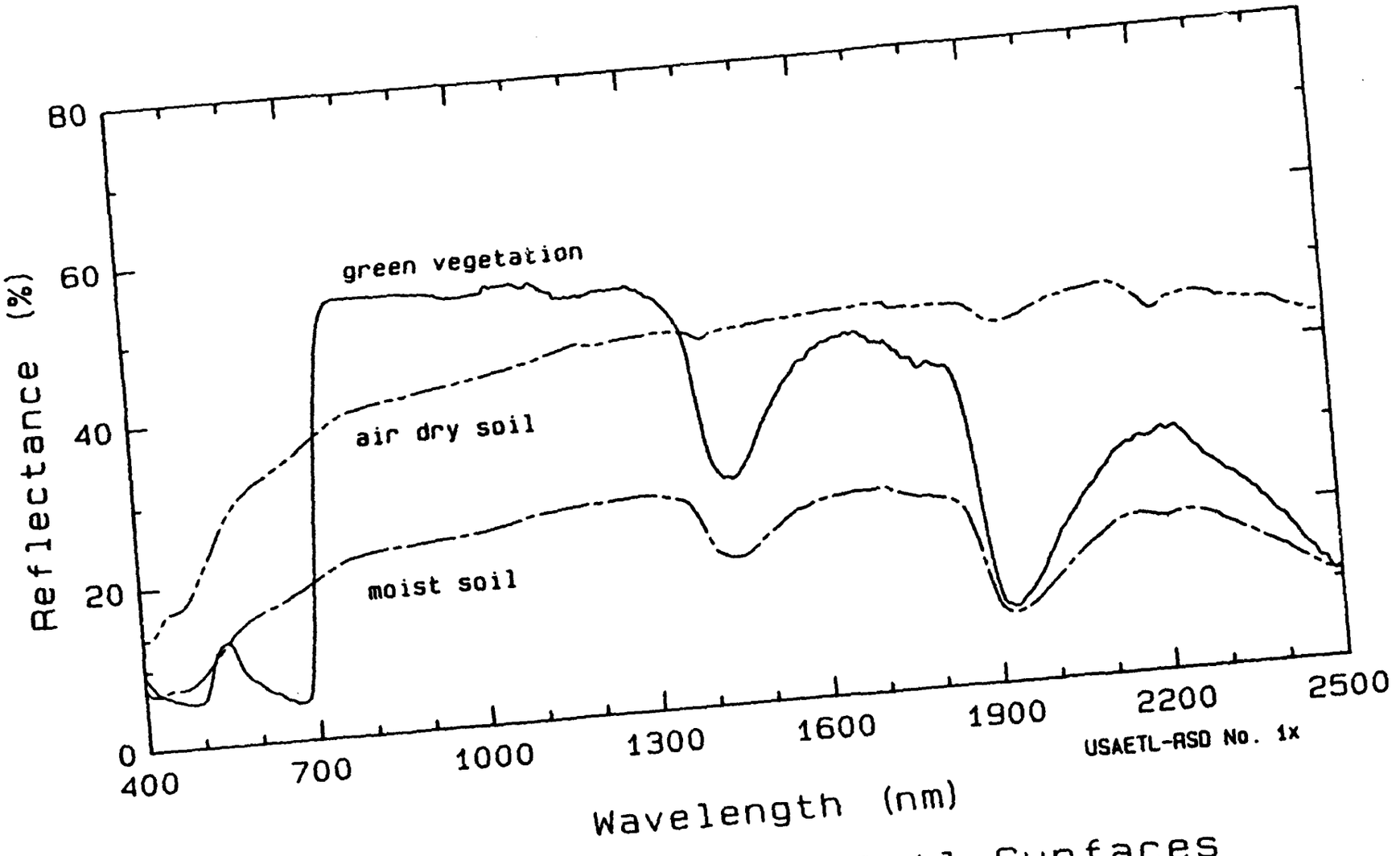

FIGURE B2. Air Dry and Moist Soil Surfaces and Green Vegetation.

Table B1. Mean Vectors of the Training Data

	B1	B2	B3	B4	B5	B6	B7
Oil H	66.34	20.52	18.11	14.37	49.85	132.66	23.37
Oil M	69.17	21.47	18.20	13.88	31.08	111.49	15.19
Oil R	68.24	21.22	18.67	12.15	17.17	136.70	12.00
Land A	135.75	70.08	103.27	89.35	153.27	123.89	105.29
Land B	137.63	66.33	92.80	76.01	122.55	126.64	77.70
WetCove	122.40	55.08	70.30	54.91	43.09	113.34	17.59
WetSand	117.54	56.80	81.32	68.41	117.78	128.64	74.37
Water A	65.82	19.43	15.00	8.91	5.00	120.35	3.90
Water B	85.73	24.90	16.97	9.76	5.96	112.03	4.52
Water C	142.64	62.83	66.02	24.09	9.72	106.82	5.64
Cloud	118.55	39.36	40.05	27.05	23.46	79.46	14.55

The mean vectors for Oil, Water A, and Water C are plotted in Figure B3, where Oil = average of (Oil H, Oil M, and Oil R).

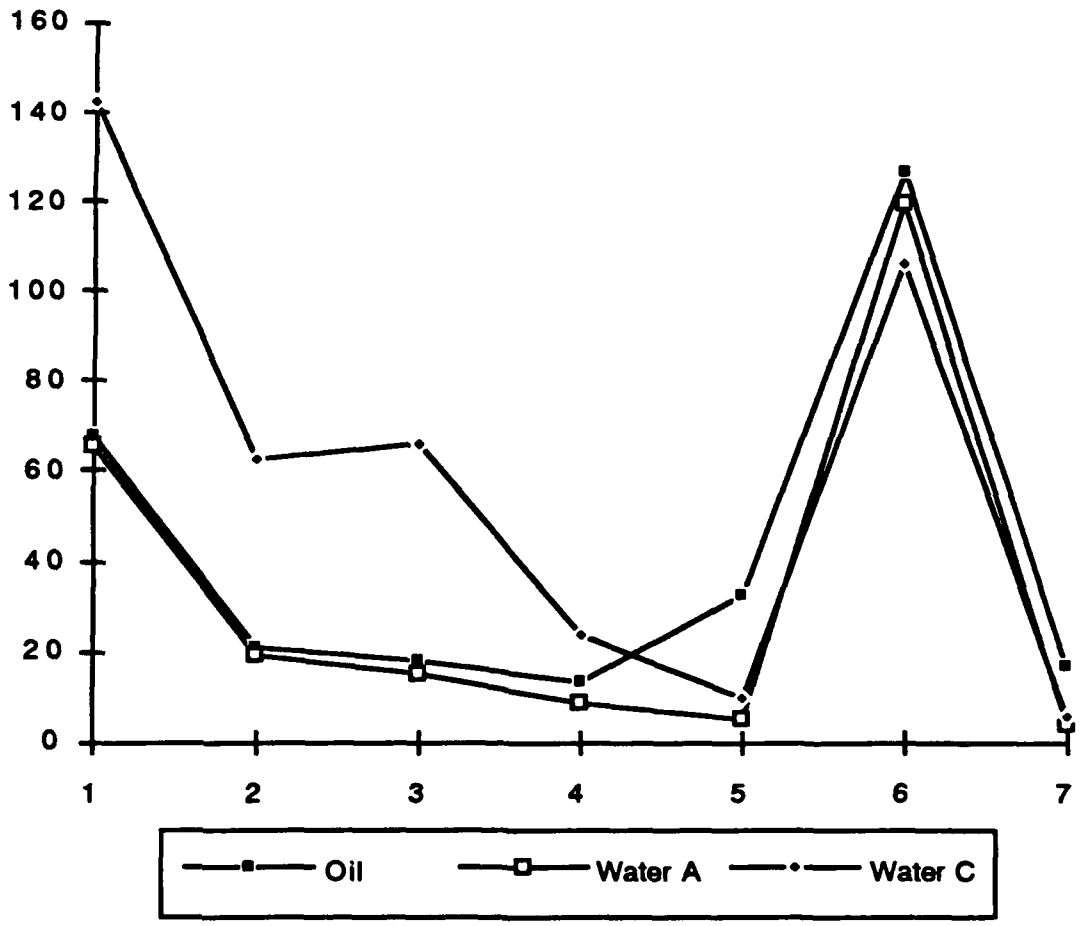

Figure B3. Landsat TM-Derived Spectral Curves of Oil and Water.

Table B2. Covariance Matrices

Oil H

	B1	B2	B3	B4	B5	B6	B7
B1	1.83	0.75	0.25	-0.21	-4.28	-3.08	-1.84
B2	0.75	0.48	0.21	-0.08	-1.76	-1.05	-0.69
B3	0.25	0.21	0.87	0.84	0.33	-0.10	-0.06
B4	-0.21	-0.08	0.84	1.38	1.91	-0.03	0.29
B5	-4.28	-1.76	0.33	1.91	23.19	13.39	11.13
B6	-3.08	-1.05	-0.10	-0.03	13.39	17.57	7.40
B7	-1.84	-0.69	-0.06	0.29	11.13	7.40	6.18

Oil M

	B1	B2	B3	B4	B5	B6	B7
B1	4.09	1.62	-0.75	-3.15	-19.84	-3.33	-8.01
B2	1.62	0.79	-0.30	-1.27	-7.93	-1.34	-3.16
B3	-0.75	-0.30	0.41	1.04	5.77	1.04	2.18
B4	-3.15	-1.27	1.04	3.81	21.63	3.91	8.29
B5	-19.84	-7.93	5.77	21.63	134.83	23.77	52.01
B6	-3.33	-1.34	1.04	3.91	23.77	5.12	9.11
B7	-8.01	-3.16	2.18	8.29	52.01	9.11	20.53

Oil R

	B1	B2	B3	B4	B5	B6	B7
B1	5.70	1.97	0.26	-0.02	-0.20	-15.77	-1.73
B2	1.97	0.89	0.16	0.08	-0.02	-5.53	-0.67
B3	0.26	0.16	1.16	0.98	0.59	1.14	0.31
B4	-0.02	0.08	0.98	1.11	1.02	1.49	0.58
B5	-0.20	-0.02	0.59	1.02	10.15	-6.10	4.84
B6	-15.77	-5.53	1.14	1.49	-6.10	58.93	2.20
B7	-1.73	-0.67	0.31	0.58	4.84	2.20	3.20

Land 1

	B1	B2	B3	B4	B5	B6	B7
B1	14.64	7.74	12.16	9.50	11.95	-0.49	7.44
B2	7.74	4.79	7.79	6.23	8.80	0.02	6.01
B3	12.16	7.79	13.89	10.92	16.43	0.35	11.82
B4	9.50	6.23	10.92	9.68	14.25	0.75	9.93
B5	11.95	8.80	16.43	14.25	25.55	2.23	18.61
B6	-0.49	0.02	0.35	0.75	2.23	1.35	1.65
B7	7.44	6.01	11.82	9.93	18.61	1.65	14.51

Table B2. Covariance Matrices (continued)

Land 2

	B1	B2	B3	B4	B5	B6	B7
B1	22.18	9.16	9.90	6.10	0.67	-8.17	-4.83
B2	9.16	4.39	5.01	3.53	2.67	-2.72	0.37
B3	9.90	5.01	6.54	4.87	5.49	-2.21	2.97
B4	6.10	3.53	4.87	4.12	5.84	-0.76	4.24
B5	0.67	2.67	5.49	5.84	15.38	3.04	15.00
B6	-8.17	-2.72	-2.21	-0.76	3.04	5.40	5.27
B7	-4.83	0.37	2.97	4.24	15.00	5.27	16.95

WetCove

	B1	B2	B3	B4	B5	B6	B7
B1	69.51	38.43	57.13	41.25	5.67	2.82	-0.66
B2	38.43	21.76	32.36	23.78	3.51	1.86	-0.47
B3	57.13	32.36	49.45	37.38	10.30	3.22	1.05
B4	41.25	23.78	37.38	31.51	17.99	3.32	4.46
B5	5.67	3.51	10.30	17.99	74.36	2.83	27.92
B6	2.82	1.86	3.22	3.32	2.83	1.11	0.78
B7	-0.66	-0.47	1.05	4.46	27.92	0.78	11.06

WetSand

	B1	B2	B3	B4	B5	B6	B7
B1	16.20	9.22	14.90	12.16	16.91	2.06	9.67
B2	9.22	5.54	8.70	7.11	9.92	1.23	5.70
B3	14.90	8.70	14.40	11.87	16.72	2.00	9.33
B4	12.16	7.11	11.87	10.09	14.12	1.56	7.70
B5	16.91	9.92	16.72	14.12	21.38	2.54	11.98
B6	2.06	1.23	2.00	1.56	2.54	0.88	1.75
B7	9.67	5.70	9.33	7.70	11.98	1.75	7.99

Water A

	B1	B2	B3	B4	B5	B6	B7
B1	0.64	0.22	0.02	-0.01	-0.01	0.03	-0.01
B2	0.22	0.26	0.00	-0.01	0.00	0.02	-0.01
B3	0.02	0.00	0.05	0.00	0.00	-0.01	0.00
B4	-0.01	-0.01	0.00	0.08	0.00	0.01	-0.01
B5	-0.01	0.00	0.00	0.00	0.02	0.00	0.00
B6	0.03	0.02	-0.01	0.01	0.00	0.31	0.00
B7	-0.01	-0.01	0.00	-0.01	0.00	0.00	0.10

Table B2. Covariance Matrices (continued)

Water B

	B1	B2	B3	B4	B5	B6	B7
B1	2.34	0.25	-0.05	-0.15	-0.04	0.22	-0.13
B2	0.25	0.19	0.01	0.00	0.00	-0.02	-0.01
B3	-0.05	0.01	0.11	0.04	0.01	-0.04	0.01
B4	-0.15	0.00	0.04	0.22	0.01	-0.09	0.02
B5	-0.04	0.00	0.01	0.01	0.04	-0.03	0.00
B6	0.22	-0.02	-0.04	-0.09	-0.03	0.61	-0.05
B7	-0.13	-0.01	0.01	0.02	0.00	-0.05	0.25

Water C

	B1	B2	B3	B4	B5	B6	B7
B1	28.58	20.49	53.95	64.85	20.92	9.06	5.73
B2	20.49	16.10	45.87	56.61	17.13	7.34	4.68
B3	53.95	45.87	149.73	201.49	60.75	25.14	16.33
B4	64.85	56.61	201.49	312.84	107.83	41.79	28.60
B5	20.92	17.13	60.75	107.83	48.27	16.65	12.94
B6	9.06	7.34	25.14	41.79	16.65	6.68	4.46
B7	5.73	4.68	16.33	28.60	12.94	4.46	3.68

Cloud

	B1	B2	B3	B4	B5	B6	B7
B1	31.50	12.17	16.88	12.83	12.41	-18.78	7.55
B2	12.17	4.81	6.55	4.98	4.83	-7.36	2.94
B3	16.88	6.55	9.38	7.00	6.74	-10.07	4.07
B4	12.83	4.98	7.00	5.47	5.07	-7.59	3.07
B5	12.41	4.83	6.74	5.07	5.12	-7.45	2.98
B6	-18.78	-7.36	-10.07	-7.59	-7.45	12.07	-4.45
B7	7.55	2.94	4.07	3.07	2.98	-4.45	1.88

APPENDIX C - Radiometric Mappings and Nomenclature

Table C1 lists the mappings used to convert the 10-bit data to 8-bit data. Table C2 lists the nomenclature used for the resultant images after the 8-bit conversion, the co-registration, and the magnification.

Table C1. Mappings for AVHRR Data (I*2 to Byte Data)

AV0116.NOON								
BAND	FROM				TO			
1	0	66	266	724	0	10	210	255
2	0	51	251	683	0	10	210	255
3	0	255	740	929	0	10	240	255
4	0	352	552	741	0	10	210	255
5	0	305	543	716	0	10	210	255

AV0124.MORN								
BAND	FROM				TO			
1	0	50	250	426	0	10	210	255
2	0	45	245	409	0	10	210	255
3	0	545	806	986	0	10	200	200
4	0	392	500	826	0	10	200	200
5	0	392	500	826	0	10	200	200

AV0201.MORN								
BAND	FROM				TO			
1	0	77	183	447	0	10	210	255
2	0	66	166	422	0	10	210	255
3	0	436	755	935	0	10	200	200
4	0	405	562	822	0	10	200	200
5	0	405	564	821	0	10	200	200

AV0201.NOON								
BAND	FROM				TO			
1	0	69	241	698	0	10	210	255
2	0	54	240	690	0	10	210	255
3	0	223	697	921	0	10	200	200
4	0	342	462	927	0	10	200	200
5	0	298	422	814	0	10	200	200

AV0208.NOON								
BAND	FROM				TO			
1	0	86	531	872	0	10	210	255
2	0	66	521	827	0	10	210	255
3	0	258	645	951	0	10	240	255
4	0	390	543	842	0	10	210	255
5	0	333	504	817	0	10	210	255

Table C2. AVHRR Images Used to Monitor the Oil Spill

	AVHRR DATA (5 BANDS 1 Km pixels)		
SOURCE IMAGE	8 BIT IMAGE	CO-REGISTERED	2X ZOOM CC
AV0116.NOON	AV0116.NOON8	AV0116.NOON8R	AV0116.NOON8C
AV0124.MORN	AV0124.MORN8	AV0124.MORN8	AV0124.MORN8C
AV0125.MORN	AV0125.MORN8	*	*
AV0201.MORN	AV0201.MORN8	AV0201.MORN8R	AV0201.MORN8C
AV0201.NOON	AV0201.NOON8	AV0201.NOON8R	AV0201.NOON8C
AV0208.NOON	AV0208.NOON8	AV0208.NOON8R	AV0208.NOON8C

* = Image not generated

Note the nomenclature to designate the origins of the subscene. For example, AV0116.NOON can be translated to AVHRR acquired on 1/16/91 at approximately NOON. As listed in Table C2, remapped subscenes were given an "8" suffix (e.g. AV0116.NOON -> AV0116.NOON8).

The AV0124.MORN8 subscene was used as the base scene for which the other four subscenes were registered. During the registration process, these four subscenes were resampled using a bilinear interpolation option. The names of these subscenes were given an additional "R" suffix (e.g. AV0116.NOON8 -> AV0116.NOON8R).

The magnified images (2XZOOMCC) were resampled using cubic convolution. As listed in this table, the names of these subscenes were given a "C" suffix (e.g. AV0116.NOON8R -> AV0116.NOON8C).

LIST OF ACRONYMS

AVHRR	Advanced Very High Resolution Radiometer
BIL	Band Interleaved by Line
CMYK	Cyan, Magenta, Yellow, and Black
CRREL	USACE Army Cold Regions Research and Engineering Laboratory
EOC	Corps of Engineers Emergency Operation Center
ERDAS	Earth Resource Data Analysis
GSL	TEC's Geographic Sciences Laboratory
IFOV	Instantaneous Field of View
ISODATA	Iterative Self-Organizing Data Analysis Techniques A
LAS	Land Analysis System
MVN	Multivariate Normal
QRMP	Quick Response Multicolor Printer
RGB	Red, Green, Blue
RI	TEC's Research Institute
RIP	Raster Input Processor
SLAR	Side-Looking Airborne Radar
SPL	TEC's Space Programs Laboratory
SRTF/MBIPS	Space Research Test Facility, Multiband Image Processing System
TDL	TEC's Topographic Developments Laboratory
TEC	U.S. Army Topographic Engineer Center
TM	Landsat Thematic Mapper